CORROSION SCIENCE AND TECHNOLOGY, Vol.3, No.3(2004), pp.87~97

Meso-Scale Approach for Prediction of Mechanical Property and Degradation of Concrete

Tamon Ueda

Division of Structural and Geotechnical Engineering, Hokkaido University, Kita-ku, Sapporo, 060-8628, JAPAN

This paper presents a new approach with meso scale structure models to express mechanical property, such as stress - strain relationships, of concrete. This approach is successful to represent both uniaxial tension and uniaxial compression stress - strain relationship, which is in macro scale. The meso scale approach is also applied to predict degraded mechanical properties of frost-damaged concrete. The degradation of mechanical properties with frost-damaged concrete was carefully observed. Strength and stiffness in both tension and compression decrease with freezing and thawing cycles (FTC), while stress-free crack opening in tension softening increases. First attempt shows that the numerical simulation can express the experimentally observed degradation by introducing changes in the meso scale structure in concrete, which are assumed based on observed damages in the concrete subjected to FTC. At the end applicability of the meso scale approach to prediction of the degradation by combined effects of salt attack and FTC is discussed. It is shown that clarification of effects of frost damage in concrete on corrosion progress and on crack development in the damaged cover concrete due to corrosion is one of the issues for which the meso scale approach is useful.

Keywords : *meso scale structure model, stress - strain relationship, degraded mechanical property, frost damage, salt attack*

1. Introduction

Concrete consists of coarse aggregate, fine aggregate, cement, water, air and admixtures. Although we deal with concrete as a homogeneous material, the reality is a heterogeneous material. Because of this fact it can be easily predicted that stresses in micro scale are quite different from the usual stress - strain relationship, which is in macro scale. We say that concrete fails in compression once stress reaches its compressive strength. In compression failure, however, we observe many cracks, which represent tension failure. Those facts imply that an approach with smaller scale is quite useful to understand deformation and strength characteristics of concrete.

In this paper an approach with meso scale is presented. This meso scale approach is based on Rigid Body Spring Model (RBSM) with element size of millimeter order and corresponding constitutive models. This approach is applied to predict stress - strain relationship under both uniaxial tension and uniaxial compression in macro scale, which is usually known as concrete material property.

Concrete with damages induced by environmental actions shows deterioration of its mechanical properties such as strength and stiffness in macro scale. Previous studies did not clarify quantitatively how much deterioration would occur in damaged concrete. Understanding damage mechanism in smaller scale could help us to predict when and how much deterioration we would have and to know what are appropriate measures to prevent or slow the deterioration.

The meso scale approach with RBSM is applied to express degraded mechanical properties of concrete. As an example, concrete subjected to freezing and thawing cycles (FTC) is chosen. In the meso scale approach the material constitutive models are changed based on experimentally observed damages due to FTC. Then, how to apply the meso scale approach to prediction of the degradation by combined effects of salt attack and FTC is discussed. It is shown that clarification of effects of frost damage in concrete on steel corrosion progress and on crack propagation in the damaged cover concrete due to the corrosion is one of the issues for which the meso scale approach is useful.

2. RBSM in meso scale[1),2)]

RBSM developed by Kawai is one of discrete numerical analysis methods.[3)] RBSM can be applied to both three-

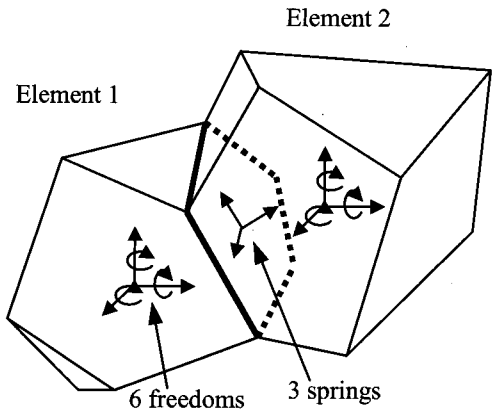

Fig. 1. Element in RBSM

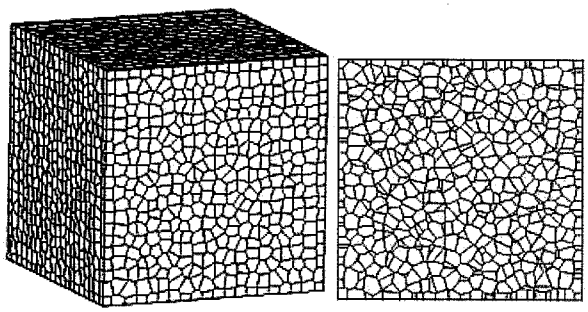

a) 3D view b) Cross section

Fig. 2. 3D Voronoi geometry

and two-dimensional problems. Here three-dimensional case is introduced. The analytical target is divided into polyhedron elements whose faces are interconnected by springs. Each element has three transitional and three rotational degrees of freedom at the center of gravity. One normal and two shear springs are placed at the centroid of each face (Fig. 1). Since cracks initiate and propagate along the boundary face, the element arrangement may affect fracture direction. To avoid formation of cracks in a certain direction, a random geometry is introduced using a three-dimensional Voronoi diagram (Fig. 2). The Voronoi diagram is the collection of Voronoi cells. Each cell represents mortar or aggregate element in the analysis.

2.1 Material model - mortar

In this study, a constitutive model for mortar in meso scale, which is in millimeter order, is developed because the constitutive model in macro scale cannot be applied to meso scale analysis.

Material characteristics of each component are presented by means of modeling springs. In normal springs, compressive and tensile stresses (σ) are developed. Shear springs develop shear stresses (τ). A resultant of strains generated in two shear springs is used as a shear strain for calculation of the corresponding shear stress. Elastic modulus of springs are presented as follows:

$$k_n = \frac{(1-\nu_{elem})E_{elem}}{(1-2\nu_{elem})(1+\nu_{elem})} \tag{1-1}$$

$$k_s = \frac{E_{elem}}{2(1+\nu_{elem})} \tag{1-2}$$

where k_n and k_s are the elastic modulus of normal and shear spring, E_{elem} and ν_{elem} are the elastic modulus and Poisson's ratio of component for meso level, respectively.

In the analysis, due to the modeling nature for RBSM, values of the material property in meso level given to the element are different from those of the analyzed object as the macroscopic material property. In this study, the material properties for the element in meso scale were determined in such a way to give the correct macroscopic properties. For this purpose, the elastic analysis of mortar in compression was carried out. In discrete analysis such as RBSM analysis, shape of elements and element fineness affect the analytical result.[4] To reduce these effects, small size for element is adopted and element finenesses in all analyses are in almost same level. Volume of each element is about 2.5~3.0 mm^3 in this study. In the elastic analyses, the relationship between the macroscopic and mesoscopic Poisson's ratio and the effect of the mesoscopic Poisson's ratio on the macroscopic elastic modulus were examined. From the results, Eq.(2) is adopted for determining the mesoscopic material properties.

$$\nu_{elem} = -237.0\nu^4 + 266.6\nu^3 - 116.1\nu^2 + 24.1\nu - 1.6 \quad (0.12 \le \nu \le 0.35) \tag{2-1}$$

$$E_{elem} = \left(-41.5\nu_{elem}^{\ 4} + 21.1\nu_{elem}^{\ 3} - 5.5\nu_{elem}^{\ 2} + 0.4\nu_{elem} + 1.3\right)E \tag{2-2}$$

where E and ν are macroscopic elastic modulus and Poisson's ratio of component of analyzed object, respectively.

Only the maximum tensile stress has to be set as a material strength. Actually, even when bleeding effect is ignored, mortar itself is not a homogeneous material, consisting of sand and paste. Strength variation in mortar has not been clarified yet. In this study, a normal distribution is assumed for the tensile strength variation of spring element. The probability density function is as follows (Fig. 3):

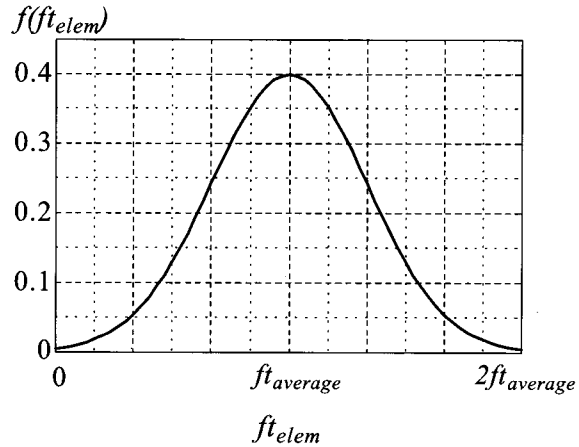

Fig. 3. Distribution of tensile strength

$$f(f_{t\,elem}) = \frac{1}{\sqrt{2\pi}} \exp\left\{ -\frac{\{3(f_{t\,elem} / f_{t\,average} - 1)\}^2}{2} \right\} \quad (3)$$

where $f_{t\ elem}$ is distributed tensile strength ($f_{t\ elem} \geq 0$) and $f_{t\ average}$ is average tensile strength of mortar in meso level. The same distribution is given to the elastic modulus. Those distributions affect the macroscopic elastic modulus, so that the elastic modulus for the element given by Eq.(2-2) is multiplied by 1.05.

Springs set on element faces act elastic until stresses reach the τ_{max} criterion or tensile strength. The strains and stresses are calculated as follows:

$$\varepsilon = \frac{\Delta n}{h_1 + h_2}, \quad \gamma = \frac{\Delta s}{h_1 + h_2} \quad (4\text{-}1)\ (4\text{-}2)$$

$$\sigma = k_n \varepsilon, \quad \tau = k_s \gamma \quad (4\text{-}3)\ (4\text{-}4)$$

where ε and γ are the strain of normal and shear springs, Δn and Δs are the normal and shear relative displacement between element boundary faces where those springs are located, and h is the length of perpendicular line from the center of gravity of the element to the boundary face. Subscripts 1 and 2 represent elements 1 and 2 in Fig. 1, respectively.

Constitutive model of normal spring is shown in Fig. 4. In compression zone, it always acts elastic. Fracture happens between elements when spring reaches tensile strength $f_{t\ elem}$, and the normal tensile stress decreases linearly depending on crack width that is the spring elongation. In this study, stress-free crack width w_{max} is set 0.005 mm. The linear unloading and reloading path that goes through the origin is introduced to normal spring

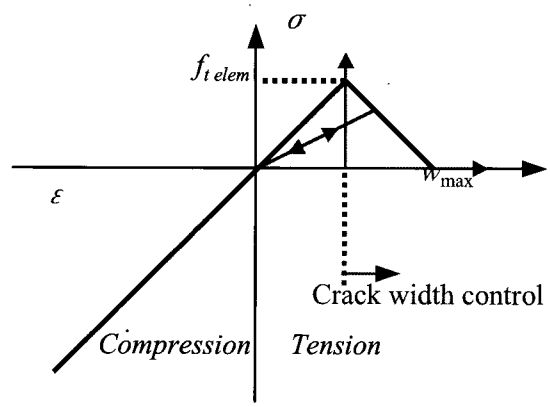

Fig. 4. Model of normal spring

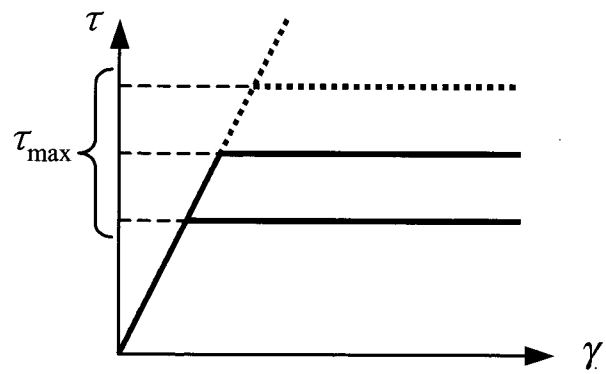

Fig. 5. Model of shear spring

in tension zone. For shear spring, elasto plastic model is applied as shown in Fig. 5 when normal spring has not fractured yet. Value of τ_{max} changes depending on the condition of normal spring and given as follows:

$$\tau_{\max} = \pm\left\{0.08 f_{telem}^{\ 2.7} (-\sigma + f_{telem})^{0.7} + f_{telem}\right\} \quad (5)$$

When the fracture happens in normal spring, the calculated shear stress is reduced corresponding to the reduction ratio of normal stress. As a result, shear spring cannot carry the stress either when crack width of normal spring reaches w_{max}.

In this study, normal springs in compression only behave elastically and never break nor have softening behavior (Fig. 4).

2.2 Material model - aggregate

In this study, it is assumed that the strength of aggregate is stronger than that of mortar. Therefore, element of aggregate behaves only elastic without fracture. Equations (1), (2), and (4) are adopted to present the material property of aggregate.

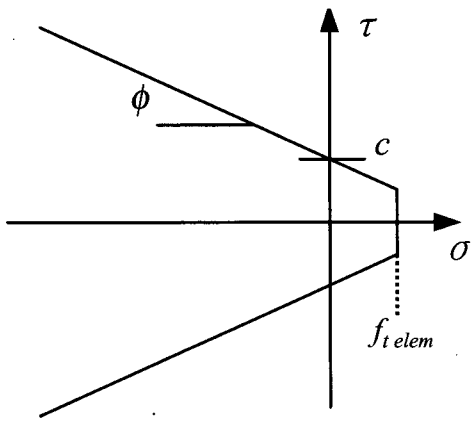

Fig. 6. τ_{max} criterion for interface

2.3 Material model - interface

The same stress-strain relationships as Eq.(4) and strength and stiffness distribution as Eq.(3) are adopted for the material properties of the interface between mortar and aggregate. The spring stiffnesses k_n and k_s (Eq.(1)) of the interface are given by a weighted average of the material properties in two elements on both sides of the interface according to their length of perpendicular line from the center of gravity of the element to the interface where the springs are set. For the interface between mortar and aggregate, the τ_{max} criterion as shown in Eq.(6) and Fig. 6 is adopted.

$$\tau_{\max} = \pm(-\sigma \tan\phi + c) \quad \text{for} \quad \sigma < f_{telem} \tag{6}$$

where Φ and c are material constants. This criterion is based on the failure criterion suggested by Kosaka et al. which is derived from experimental results.[5] After stresses reach the failure criterion, the shear stress (τ) is reduced to τ_{max} which depends on the normal stress (σ) in the range where the normal stress is in compression. In the tension stress range, both normal and shear springs cannot transfer stresses once the stresses reach the criterion.

3. Prediction of mechanical property by RBSM in meso scale

3.1 Behavior in tension

A mortar prism as shown in Fig. 7 is analyzed. Material constants are given in Table 1. Fig. 8 shows stress - strain relationship in macro scale of the prism subjected to uniaxial tension. The predicted relationship agrees reasonably with experimental one. The tensile strength in macro scale is 4.47 MPa, while that in meso scale is 4.20 MPa. Deformation at failure, where tensile stress in macro scale is almost zero, is shown in Fig. 9. Propagation of a single crack in macro scale is seen as in experiment.

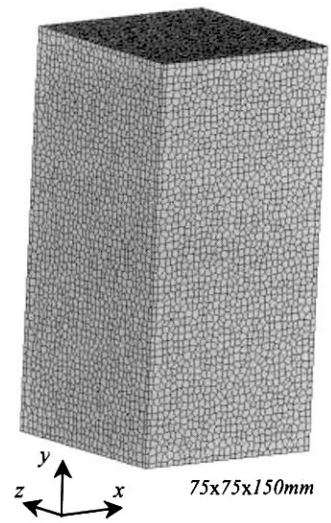

Fig. 7. Mortar prism

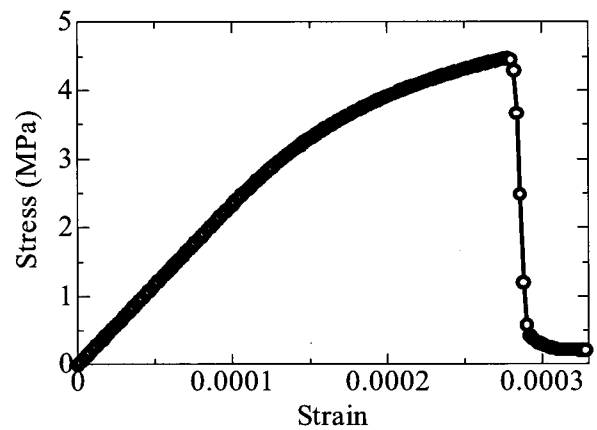

Fig. 8. Stress-strain curve in tension

Table 1. Input material properties for meso scale

Mortar		
$f_{t\ average}$	Elastic modulus (E)	Poisson's ratio (ν)
4.2 MPa	24,000 MPa	0.18
Aggregate		
Elastic modulus (E)	Poisson's ratio (ν)	
50,000 MPa	0.25	
Interface		
$f_{t\ average}$	c	ϕ
1.6 MPa	2.7 MPa	35°

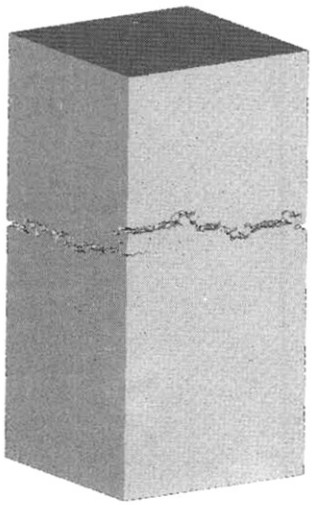

Fig. 9. Deformation at failure in tension

3.2 Behavior in compression

Mortar and concrete prisms shown in Fig. 10 are analyzed to examine compression behavior. The material constants are as shown in Table 1. Volume fractions of aggregate are 18% and 34% in the concrete prisms. Two cases for conditions of aggregate - mortar interface are analyzed; one with bond, which is represented by Eq.(6) and the other without bond, where no tensile and shear stresses are transferred. Fig. 11 presents stress - strain relationship in macro scale for the mortar prism and two concrete prisms with the two types of interface modeling cases. The peak stress of the mortar specimen, whose tensile strength is 4.47 MPa, is nearly 40 MPa. The compressive strength in macro scale decreases with the volume fraction of aggregate, while the macro-scale initial compressive stiffness increases with aggregate inclusion. Greater reduction is found in the case of prisms without interface bond. The predicted reduction in the compressive strength is quite similar to that found in experiment[6] (Fig. 12). Deformation at axial compressive strain of 2000 μ is shown in Fig. 13. Typical diagonal cracks in macro scale can be seen as in experiment.

3.3 Relationship between tensile and compressive strength

Using two-dimensional analysis by RBSM with meso scale is conducted to represent the relationship between tensile and compressive strength of concrete in macro scale. The constitutive models in meso scale are similar to those for the three-dimensional analysis but not identical. Fig. 14 shows the analyzed concrete specimen. The average element size is 3.8 mm^2 and the number of elements is 5269. The volume fraction of aggregate is 37.9%. The predicted relationship agrees quite well with

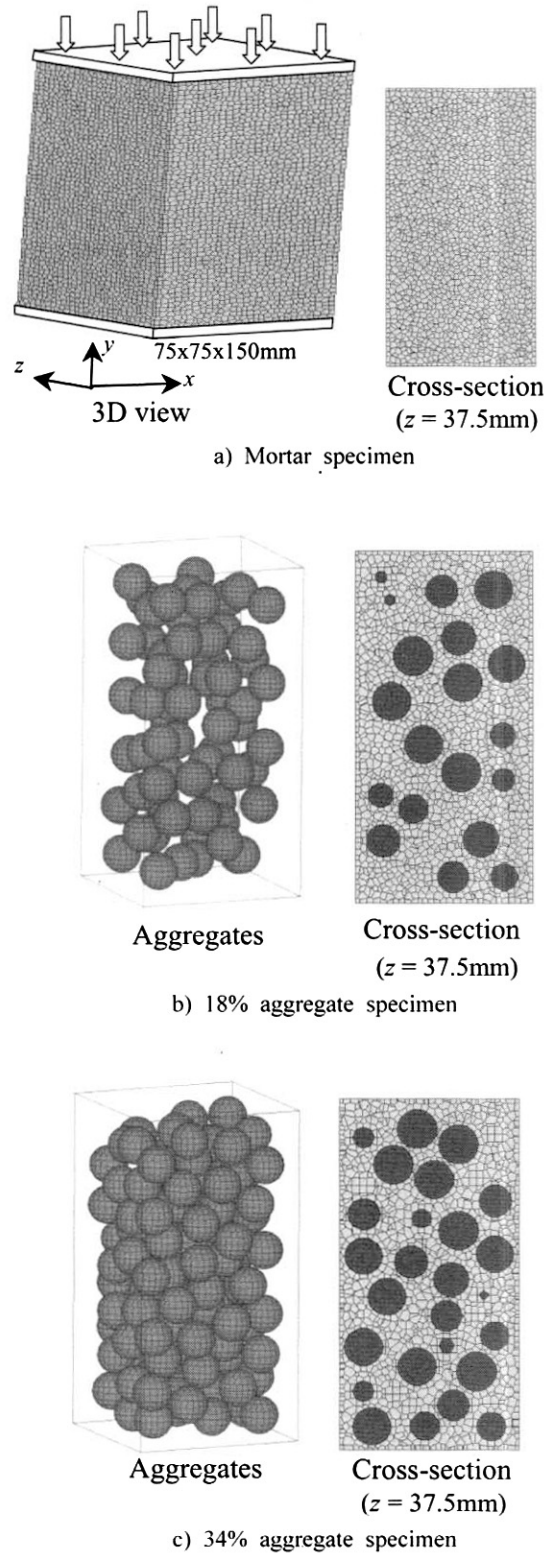

Fig. 10. Analytical specimens

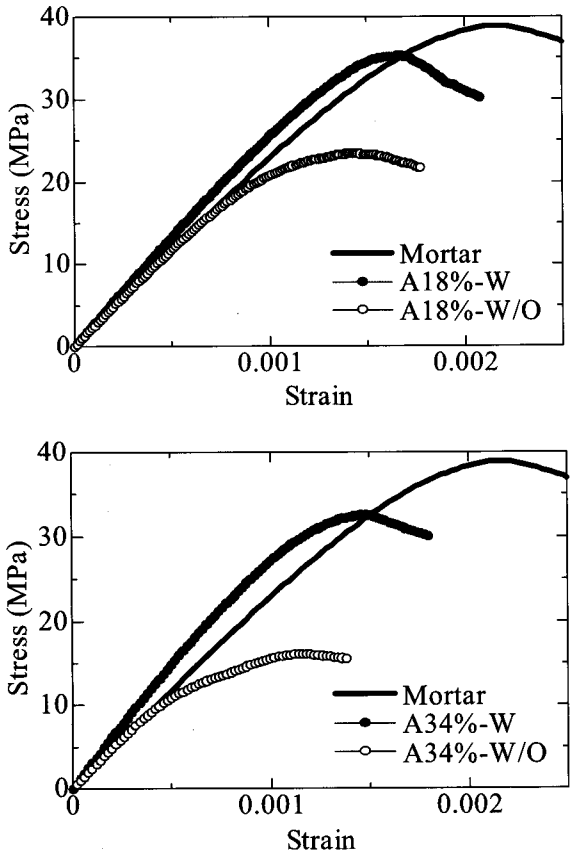

Fig. 11. Predicted stress – strain curves

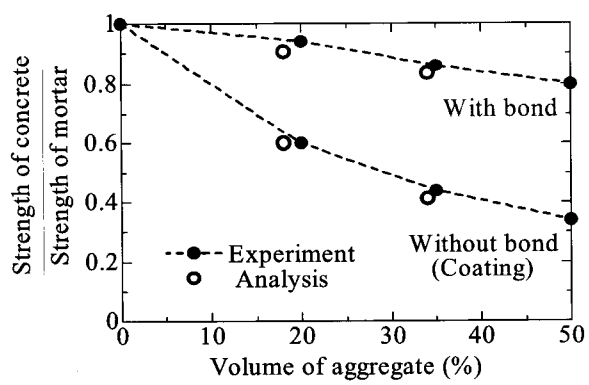

Fig. 12. Strength reduction of concrete

experimental relationship as shown in Fig. 15.[7)]

4. Prediction of mechanical property degradation in frost-damaged concrete by RBSM in meso scale[8)]

4.1 Experiment for frost damage in concrete

Freezing and thawing cycle test of concrete was conducted in water with the ASTM method (test procedure

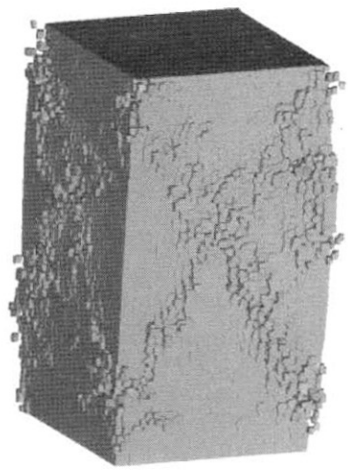

Fig. 13. Deformation at failure(Specimen A18%-W)

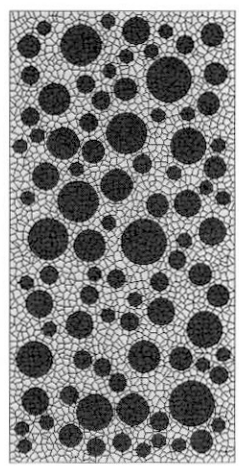

Fig. 14. Analyzed concrete specimen

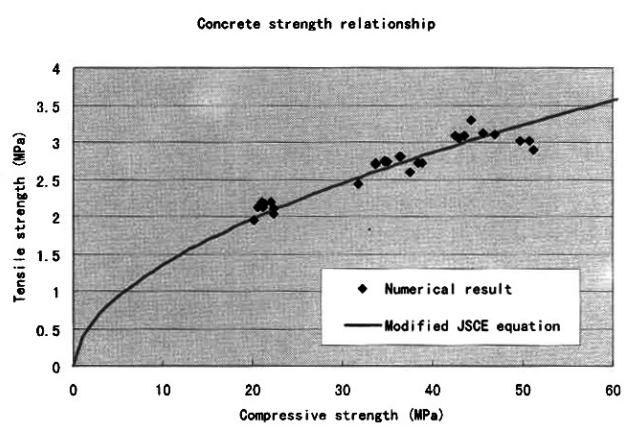

Fig. 15. Predicted relationship between compressive and tensile strength

A) or in air in a climate chamber in which temperature and moisture can be controlled and mechanical loading test can be conducted (test procedure B) (Fig. 16). The tested specimens were cylinders and prisms. The details of specimens are shown in Table 2. The maximum and minimum temperatures during freezing and thawing cycles were 20℃ and -25℃ respectively. When the input temperature reached 19℃ during thawing, water was sprayed on the specimens for 15 minutes. Strains were measured by strain gages attached on the specimen surface and embedded in the specimen (Fig. 17).

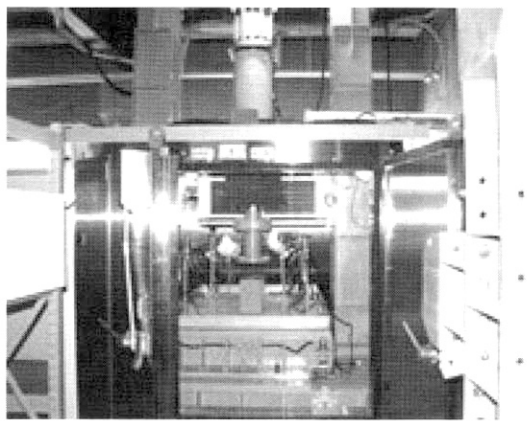

Fig. 16. Climate chamber

Table 2. Details of specimens for FTC

Series	w/c	AE agent (%)	Type	Size (cm)	TP	AT (days)
BN	0.5	0.00	Prism	10×10×40	A	30
BA	0.5	0.05	Prism	10×10×40	A	30
CN	0.5	0.00	Cylinder	ϕ 10×20	B	50
CA	0.6	0.25	Cylinder	ϕ 10×20	B	300
BEN	0.5	0.00	Prism	10×10×40	B	50

* w/c is water to cement ratio by weight. AE agent is AE agent to cement ratio by weight. TP is test procedure. AT is age of specimen when FTC test started.

4.2 Effects of frost damage on mechanical properties

It is observed in the specimens that residual (plastic) tensile strain in macro scale occurs and increases with number of freezing and thawing cycles (FTC). The plastic tensile strains are induced in both axial and lateral directions of the specimen. Fig. 18 shows the increment of plastic tensile strain in the concrete specimens tested in this study. The equivalent plastic tensile strain, which is a strain invariant and a function of axial and lateral plastic strains (ε_{pa} and ε_{pl}), is used to represent plastic deformation in the specimen. The equivalent plastic strain (E_{pf}) is defined as follows:

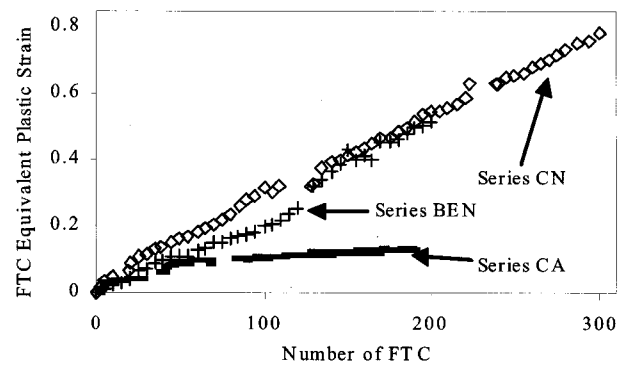

Fig. 18. Increment of plastic tensile strain

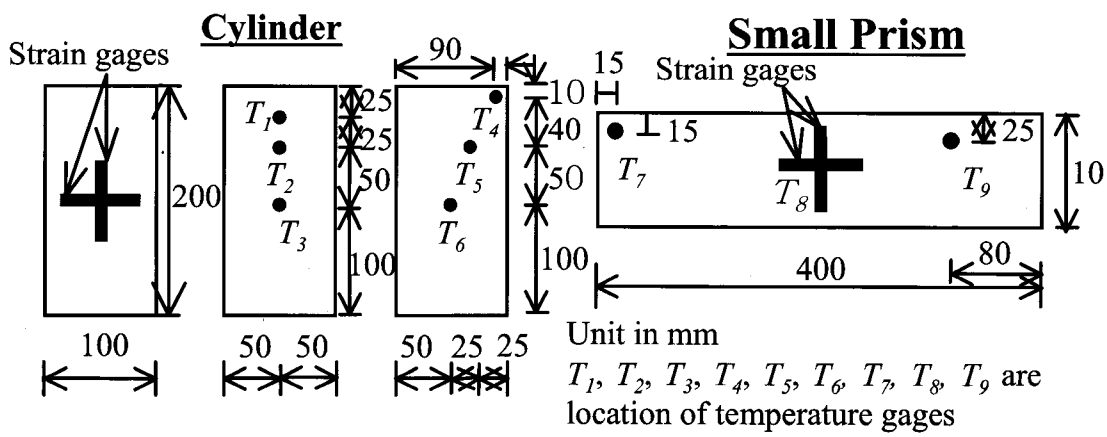

Fig. 17. Location of strain and temperature gages for cylinder and small prism specimens

$$E_{pf}=\sqrt{\left(\frac{0.31\sqrt{2}}{\varepsilon'_{co}}\left(\varepsilon_{pl}+\varepsilon_{pa}\right)\right)^2+\left(\frac{0.49\sqrt{2}}{\varepsilon'_{co}}\left(\varepsilon_{pl}-\varepsilon_{pa}\right)\right)^2} \quad (7)$$

where ε'_{co} is compressive strain of concrete at uniaxial strength and assumed to be 0.002.

As a result of damage of concrete during frost cycles, the mechanical properties such as strength and stiffness deteriorate. Fig. 19 shows the degradation of compressive strength (f'_c), static elastic modulus in compression (E_c), tensile strength (f_t) and dynamic elastic modulus (d_f) of concrete as a function of equivalent plastic tensile strain (E_{pf}) resulting from frost cycles damage. The tensile strength and dynamic elastic modulus is still same as original concrete up to the equivalent plastic tensile strain of 0.2 and reduces for the following increasing of equivalent plastic strain. Reason for the difference in degradation nature between compression and tension has not been able to be explained yet.

4.3 Prediction of degradation in mechanical property

Two-dimensional analysis is conducted to predict the degradation in macro scale of concrete strength and stiffness both in tension and compression under the effect of FTC as well as the change in stress-strain curve in macro scale. The analyzed model is mortar whose dimension is 100 mm × 200 mm as shown in Fig. 20. The number of meshing elements is 3046 and the average size of element is 6.6 mm^2.

The deterioration of concrete property caused by FTC as described in the previous section is considered by introducing zero strength elements since the fracturing elements have no ability to carry stress. Figs. 21 (a) and (b) show the reduction on strength and stiffness in tension and compression as increasing the number of zero strength elements. The results indicate the proportional reduction of tensile strength and its stiffness. It corresponds with the reduction of tensile strength and stiffness obtained by the experiment, which shows similar reduction percentage for the same plastic tensile strain (Fig. 19 (b)).

Fig. 21 (b) shows that reduction of strength is higher than that of stiffness in compression. This stiffness degradation is only caused by fracture of element. It is considered, however, that further degradation of compressive initial stiffness is possible because of plasticity induced during FTC. The initial plastic tensile strain needs to be introduced in the meso-scale model in addition to the zero strength elements.

Another factor affecting the strength and stiffness reduction is the change in tension softening at a crack, which was observed in the experiment. The maximum

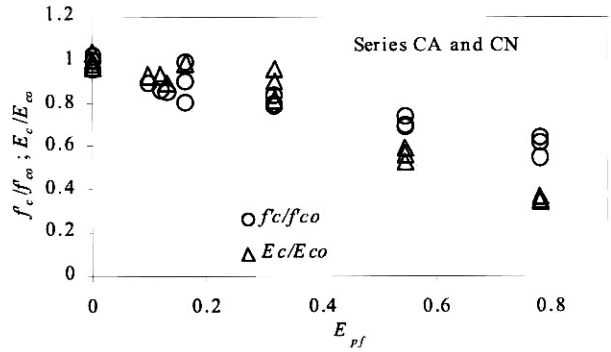

(a) Reduction of compressive strength and stiffness as a function of FTC equivalent plastic strain

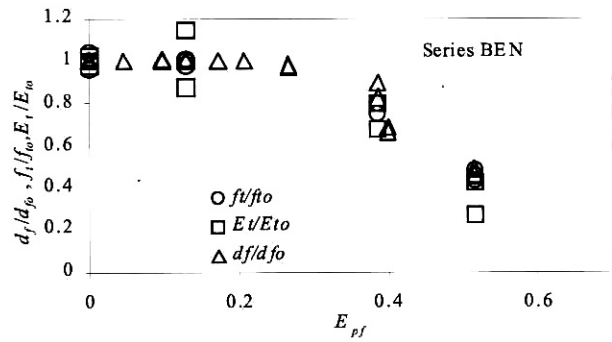

(b) Reduction of relative dynamic elastic modulus, tensile strength and stiffness as a function of FTC equivalent plastic strain

Fig. 19. Degradation of mechanical properties

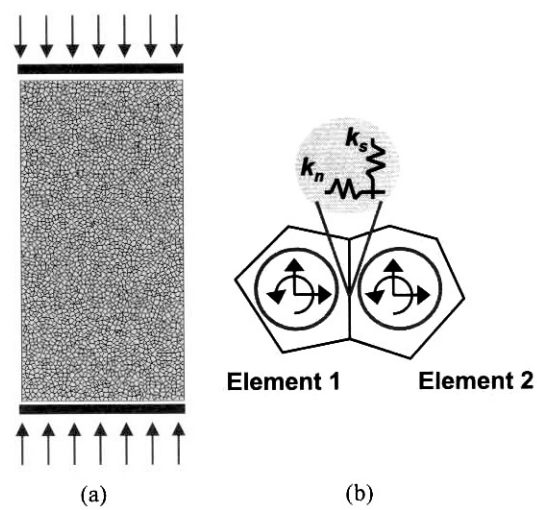

Fig. 20. Analyzed model; (a) Meshing of analyzed model; (b) RBSM polygonal elements interconnected by springs and degrees of freedom (DOF)

crack width w_{max}, at which concrete tensile stress is totally released, was observed to increase with FTC (Fig. 22).

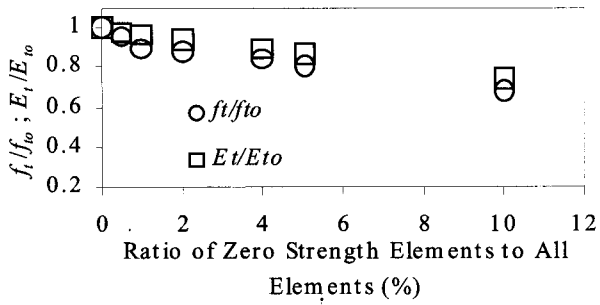

(a) Reduction of tensile strength and stiffness as increasing the number of zero strength elements at $w_{max} = 0.03$ mm

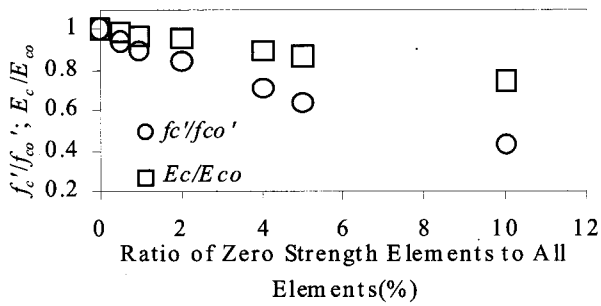

(b) Reduction of compressive strength and stiffness as increasing the number of zero strength elements at $w_{max} = 0.03$ mm

Fig. 21. Predicted deterioration of material properties

The increase in w_{max} increases in strength but stiffness (Fig. 23). It is believed that the combined effects of zero strength element, plastic tensile strain and increase in w_{max} could express the observed degradation in strength and stiffness in compression and tension. The results of further analysis will be presented in the near future

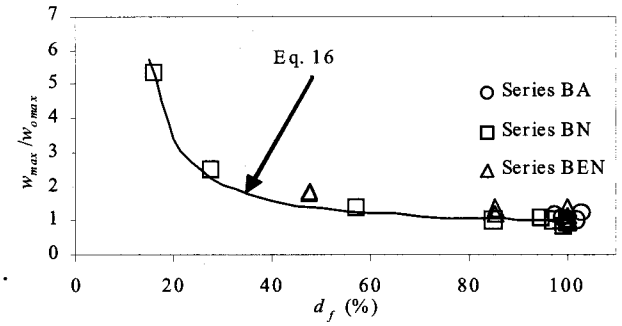

Fig. 22. Increase in stress-free crack opening (w_{max}) under FTC

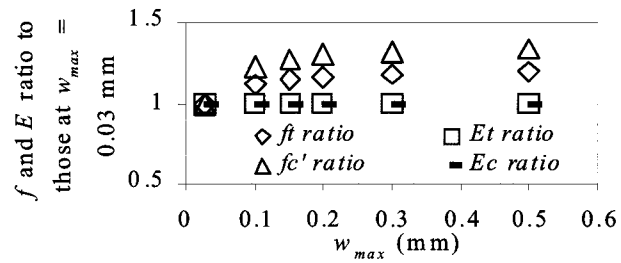

Fig. 23. Effect of stress-free crack opening (w_{max}) on mechanical properties

5. Degradation due to combined effects of salt attack and frost damage and meso scale approach

Combined effects of salt attack and freezing and thawing cycles (FTC) are a very likely cause of degradation in concrete property for structures near seacoast and highway structures. Deicing agent for keeping better load surface often contains chloride ion and causes salt attack for highway structures. For both salt attack and FTC, impermeability of concrete is a key factor to resist the

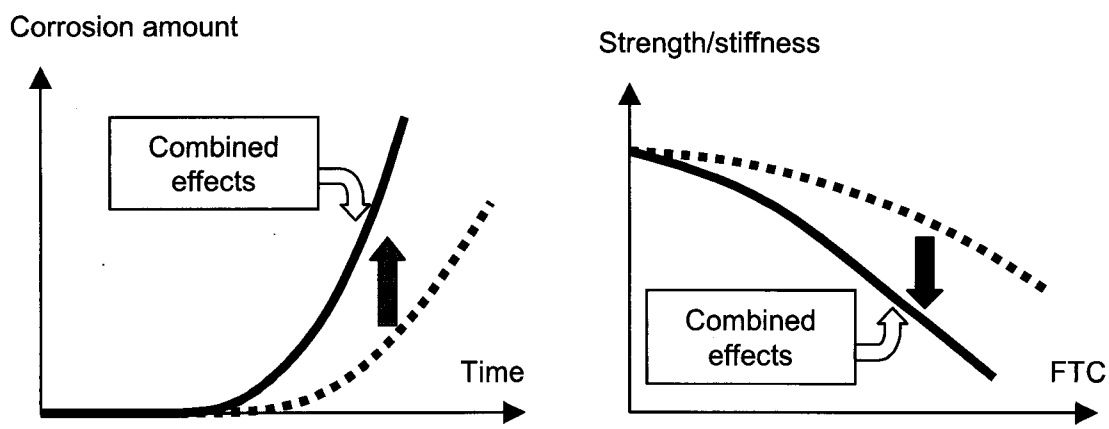

Fig. 24. Combined effects of salt attack and freezing and thawing cycles

degradation. Chloride ion penetration and water penetration are a key factor for steel corrosion due to salt attack and concrete damage due to FTC, respectively. Furthermore, both steel corrosion, which may cause cracking in cover concrete, and concrete damage due to FTC impair concrete impermeability. This means that in the case of combined effects salt attack and FTC can be a more progressive cause of degradation to each other than in the case of sole effect of either salt attack or FTC (Fig. 24).

Impermeability may be closely related to density of micro cracks, which may be represented by crack density even in meso scale (Fig. 25). The meso-scale crack density under not only the sole effect of salt attack or FTC but also combined effects of those can be numerically estimated by RBSM with meso scale modeling. Cracking in frost-damaged cover concrete due to steel reinforcement corrosion can be easily simulated by the meso-scale RBSM (Fig. 26). FTC cause not only reduction of macro-scale strength and stiffness in both tension and compression but also changes in tension softening curve in macro scale. More importantly FTC cause plastic tensile deformation in concrete. Those changes in concrete property affect macro-scale crack propagation due to steel corrosion. The meso-scale RBSM can represent numerically those changes in the concrete so as to predict precisely macro-scale cracking of the concrete with those changes.

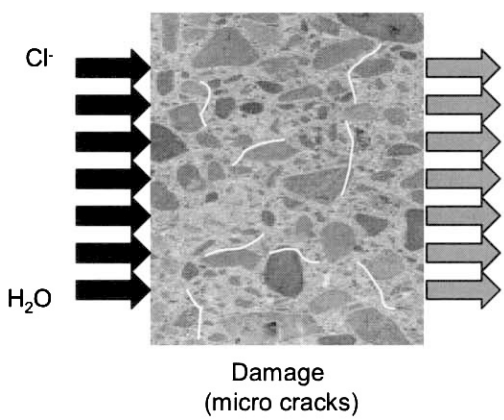

Fig. 25. Impermeability and micro cracks (damages)

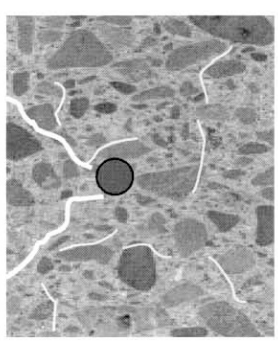

Fig. 26. Cracking in frost-damaged concrete due to corrosion

In order to predict degradation of structural performance, such as load-carrying capacity and deformability to assure safety and stiffness and cracking control capability for serviceability, the degradation of material property has to be accurately predicted. It would take a quite some time to collect experimental data for the material degradation. It is usually difficult to obtain reliable data due to complexity to model actual environmental actions such as salt attack and FTC. Since numerical approach such as meso-scale RBSM can simulate effects of environmental actions on material properties, it is a great help to reduce the experimentation time and to create environmental conditions close to the actual ones.

6. Conclusions

(1) Numerical approach with Rigid Body Spring Model (RBSM) with meso scale can simulate mechanical property of concrete in macro scale, such as tensile and compressive strength.

(2) The meso-scale RBSM can express mechanical degradation in frost-damaged concrete, such as strength and stiffness in both compression and tension by introducing fracture, increase in stress-free crack width w_{max}, and so on.

(3) It can be considered that numerical approach with meso-scale modeling is an efficient tool to predict material property degradation under the combined effects of salt attack and freezing and thawing cycles.

Acknwledgements

The author would like to express his gratitude to Dr Yasuhiko Sato, Dr Muttaqin Hasan and Mr Kohei Nagai of Hokkaido University who contributed significantly to the studies presented in this paper.

References

1. K. Nagai, Y. Sato, and T. Ueda, *Proceedings of the Japan Concrete Institute*, JCI (submitted).
2. K. Nagai, Y. Sato, and T. Ueda, *J. Str. Eng.*, JSCE, (to be printed).
3. T. Kawai and N. Takeuchi, Discrete Limit Analysis Program, Series of Limit Analysis by Computer 2, Baifukan, 1990 (in Japanese).
4. K. Nagai, *Numerical Simulation of Fracture Process of*

Concrete Model by Rigid Body Spring Method, Master Thesis submitted to Hokkaido University, 2002.
5. Y. Kosaka, H. Tanigawa, and M. Kawakami, *Proceedings of Architectural Institute of Japan*, AIJ, **228**, 1 (1975) (in Japanese).
6. P.N. Christensen, and T.P.H. Nielsen, *ACI Journal*, ACI, **66**(1), 69 (1969).
7. Concrete Committee of JSCE, *Standard Specification for Concrete Structures*, JSCE, 2002 (in Japanese).
8. T. Ueda, M. Hasan, K. Nagai, and Y. Sato, *Proceedings of FRAMCOS-5*, 2004 (to be printed).